Supplementary Figures

Supplementary Figure 1. Distribution of βGal$^+$BrdU$^+$GABA$^-$ neurons in the cerebral cortex and confirmation of the glutamatergic neuronal fate of most *Dbx1*-derived cells in the CP of P0 *Dbx1^{CRE};Tau^{GFPiresLacZ}* animals. ***A-D***, Nissl staining on P0 coronal sections shows that layer V corresponds to bins 5 to 7 (red boxes in ***B***,***D***) when dividing the dorsolateral cortex into 10 bins at both rostral (***A***,***B***) and caudal (***C***,***D***) levels (see Materials and Methods). ***E***, Graph shows the distribution of βGal$^+$BrdU$^+$GABA$^-$ neurons (expressed as the percentage of total βGal$^+$GABA$^-$ cells) into 10 bins from the MZ (left) to the SP (right) depending on the stage of BrdU injection (E10.5, E11.5, E12.5, E14.5 and E16.5; means of 3 sections per embryo ± s.e.m, at dorsolateral levels). The dashed red box shows the position of layer V. ***F,F'***, Immunohistochemistry for NeuN and Olig2 on P0 *Dbx1^{CRE};Tau^{GFPiresLacZ}* animals shows that almost all βGal$^+$ neurons express NeuN (white arrowheads) and none express Olig2, confirming their neuronal identity. ***G-G"***, Triple immunostaining for βGal, GABA and glutamate was used to control that the glutamate immunostaining does not label *Dbx1*-derived GABAergic cells (black arrowheads) whereas the βGal$^+$GABA$^-$ neurons are Glu$^+$ (white arrowheads). Scale bars: ***A***,***C***, 500µm; ***B***,***D***, 100µm; ***F,*** 20µm; ***G,*** 10µm.

Supplementary Figure 2. Migration of glutamatergic *Dbx1*-derived neurons into the dorsolateral pallium of *Dbx1^{CRE};Tau^{GFPiresLacZ}* and *Dbx1^{CRE};ROSA26^{YFP}* embryos. ***A***,***B***, *Dbx1*-derived neurons are observed in the pallium of *Dbx1^{CRE};Tau^{GFPiresLacZ}* embryos on E13.5 coronal sections stained using XGal reaction and GFP immunohistochemistry, migrating tangentially either through the IZ (black arrowhead in ***B***) or through the MZ and SP. Some radially migrating *Dbx1*-derived neurons are also observed in the developing CP (white arrowhead in ***B***). ***C-D'***, Immunostaining for YFP (***C-D***) and Tbr1 (***C-D'***) on coronal sections of E14.5 *Dbx1^{CRE};ROSA26^{YFP}* embryos labels *Dbx1*-derived glutamatergic neurons (white arrowheads in ***D***,***D'***) and shows their migration through the IZ, similar to the interneuron migration (black arrowheads) also described in Figure 4. Some YFP$^+$Tbr1$^+$ neurons are observed invading the CP by radial migration (***C',D***). Scale bars: ***A***, 100µm; ***B***,***C,*** 50µm; ***D***, 20µm.

Supplementary Figure 3. Evaluation of cell density and confirmation of the kinetic of *Dbx1*-derived cells loss using *Dbx1^{CRE};ROSA26^{YFP}* animals. ***A-D***, Cell density in the CP at E16.5, E18.5 (***A***), P0 (***B***), P2 and in layers II-VI in adults (***C***) evaluated by counting DAPI staining in 12-18 representative boxes of 100µm^2 picked randomly from 5 slices of 35µm thickness. The progressive decrease in cell density with time was observed on confocal images of DAPI staining (***A-C***) and quantified in the graph as DAPI$^+$ nuclei/mm^2 (***D***). ***E-H***, Immunohistochemistry for YFP on coronal sections of P0 (***E***,***F***) and adult (***G***,***H***) *Dbx1^{CRE};ROSA26^{YFP}* animals. ***F***,***H***, High magnifications of boxed areas in (***E***) and (***G***), respectively. ***I***, Graph shows the proportion of YFP$^+$ cells relative to DAPI$^+$ nuclei. Despite a large proportion of *Dbx1*-derived glial cells (35%, data not shown), the *ROSA26^{YFP}* reporter line presents less than half of labeled cells compared with the *Tau^{GFPiresLacZ}* reporter line, likely due to changes in recombination efficiencies. Moreover, cell loss starts at E18.5 in *Dbx1^{CRE};ROSA26^{YFP}*, probably due to the death of *Dbx1*-derived glial cells. ***J***, Coexpression of Olig2 (red) and YFP (green) shows that *Dbx1*-derived oligodendrocytes migrate in the IZ starting at E16.5. No oligodendrocytes are observed in the CP at this stage. ***K***, High magnification of (***J***) showing YFP$^+$Olig2$^+$ cells in the IZ of the dorsolateral cortex. Results are expressed as mean±s.e.m. Scale bars: ***E***,***G***, 500µm; ***F***,***H***, 300µm; ***J***, 50µm; ***K***, 20µm.

Supplementary Figure 4. Specific ablation of *Dbx1*-derived cells. ***A-F***, Tunel staining together with immunostaining for βGal on E14.5 *Dbx1^{DTA};Dbx1^{nlsLacZ}* control animals (***A***) or *E1-Ngn2/CRE;Dbx1^{DTA};Dbx1^{nlsLacZ}* triple mutant animals (***B***) show that cell death is specifically located at the level of the PSB in mutant (***F***) and no cell death is observed in the dorsolateral cortex (***D***). Moreover no Tunel staining is observed at the PSB (***E***) or in the dorsolateral pallium (***C***) of control animals. Higher detection in the green channel in (***B***) is due to residual live GFP from the *E1-Ngn2/CRE(iresGFP)* transgene. ***G-J***, XGal staining on coronal sections of E14.5 *Dbx1^{DTA};Dbx1^{nlsLacZ}* control (***G-H'***) and *E1-Ngn2/CRE;Dbx1^{DTA};Dbx1^{nlsLacZ}* triple mutant (***I-J'***) animals labeling *Dbx1*-derived cells from the PSB. ***G'***,***H'***,***I'***,***J'***, High magnifications of boxed regions in ***G***,***H***,***I*** and ***J*** respectively. A specific decrease in XGal$^+$ cells is observed in the CP of mutant animals compared with controls in both rostrodorsal (***G'***,***I'***) and caudolateral (***H'***,***J'***) regions. ***K-N***, Graphs show the number of XGal$^+$ cells in both rostrodorsal (***K***, E12.5: p=0.1296, n=171 in control and n=129 in mutant; ***M***, E14.5: p=0.0129, n=151 in control and n=90 in

mutant) and caudolateral (***L***, E12.5: p=0.036, n=650 in control and n=461 in mutant; ***N***, E14.5: p=0.0237, n=471 in control and n=245 in mutant) regions of E12.5 (***K***,***L***) and E14.5 (***M***,***N***) control and mutant developing cortices. *P<0.05, *t test*. Scale bars: ***A***,***G***,***H***,***I***,***J***, 200µm; ***G'***,***H'***,***I'***,***J'***, 50µm; ***C***, 40µm.

Supplementary Figure 5. Ablation does not affect the generation and migration of *Dbx1*-derived CR cells and interneurons or gene expression at the PSB. ***A-D***, *In situ* hybridization for *Reln* on E11.5 control (***A***,***C***) and *E1-Ngn2/CRE;Dbx1*^{DTA} (***B***,***D***) embryos at both rostral (***A***,***B***) and caudal (***C***,***D***) levels confirming the presence and normal distribution of CR neurons. ***E-G,*** Graphs show the number of *Reln*$^{+}$ cells in the dorsal/dorsolateral pallium (pink dashed boxes) of E11.5 (***E***) and E12.5 (***G***) embryos and in the medial pallium (blue dashed box) of E11.5 embryos (***F***) in both control (black bars) and mutant (green bars) telencephalons. No significant difference is observed in any regions at both stages. ***H-O***, E12.5 coronal sections of control (***H***,***J***,***L***,***N***) and *E1-Ngn2/CRE;Dbx1*^{DTA} (***I***,***K***,***M***,***O***) telencephalons were hybridized with *Ngn2* (***H***,***I***), *Dlx1* (***J***,***K***), *Wnt7b* (***L***,***M***) and *Sfrp2* (***N***,***O***) mRNA probes. No difference is observed between control and mutant animals for the expression of each of these genes. ***P***,***Q***, Immunohistochemistry for Calbindin on E12.5 control (***P***) and mutant (***Q***) embryos shows no defect in interneuron generation and migration from subpallial sources into the cortex upon ablation. ***R-U***, E14.5 coronal sections of control (***R***,***T***) and *E1-Ngn2/CRE;Dbx1*^{DTA} (***S***,***U***) telencephalons were hybridized with *TGF*α (***R***,***S***) and *Sfrp2* (***T***,***U***) RNA probes. No difference is observed between control and mutant animals. Scale bars: ***R-U***, 200µm; ***A***, ***H-Q***, 100µm.

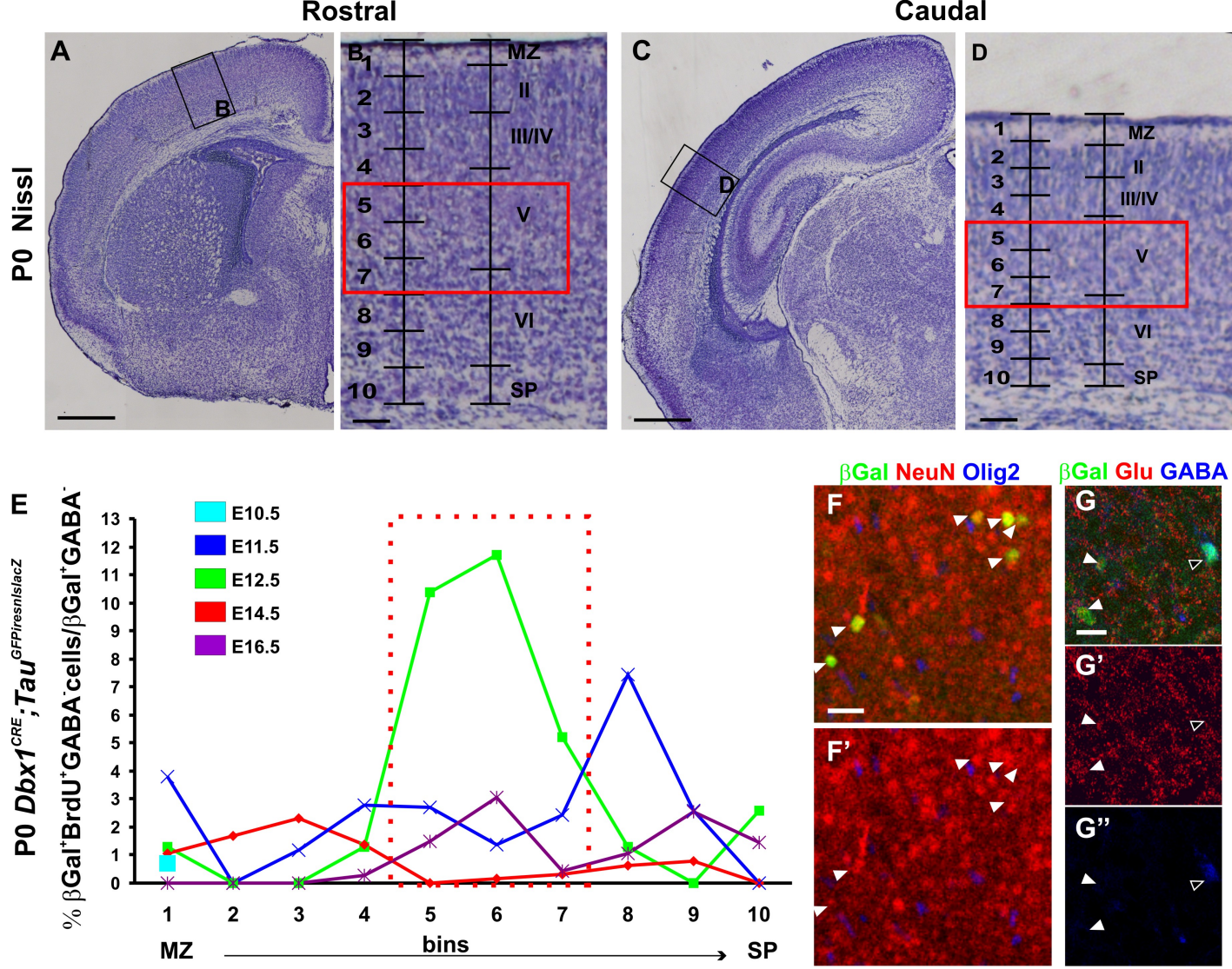

Teissier & al., Supplementary Figure 1

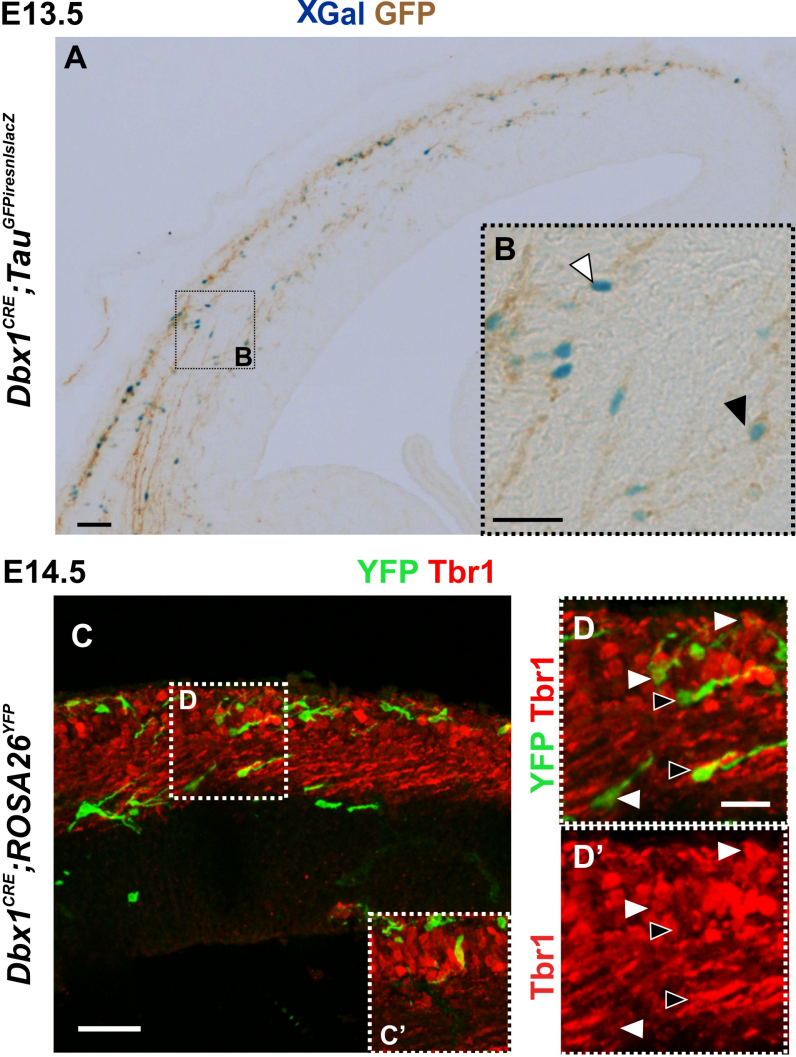

Teissier & al., Supplementary Figure 2

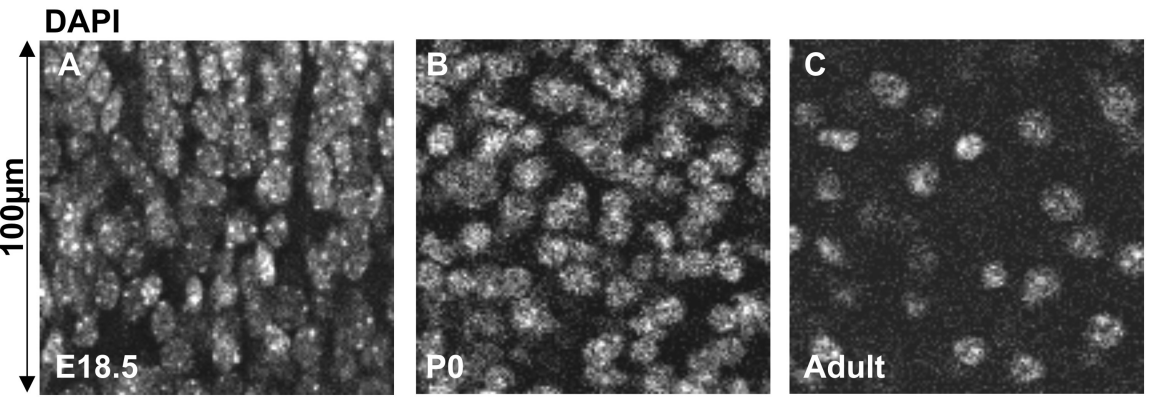

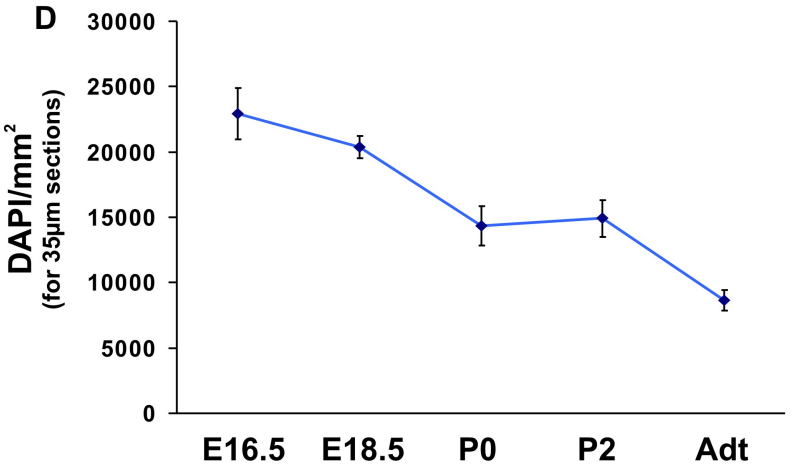

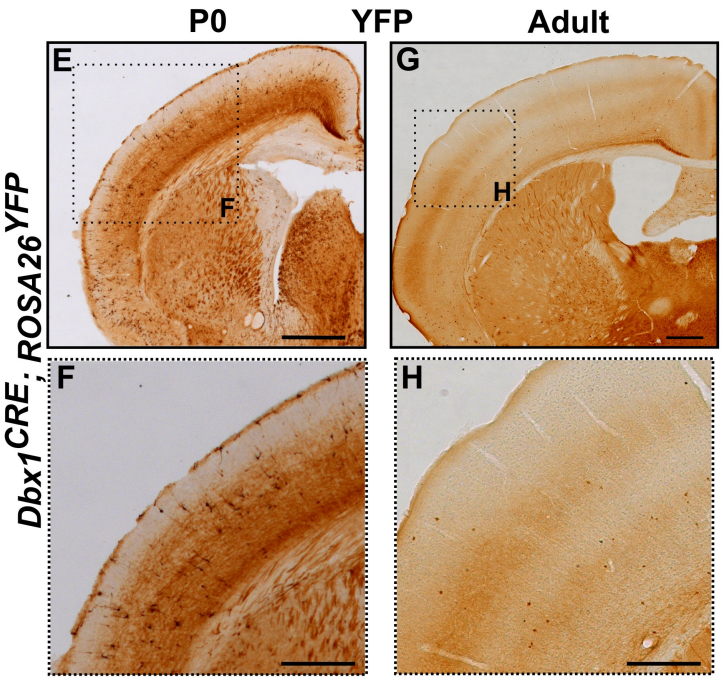

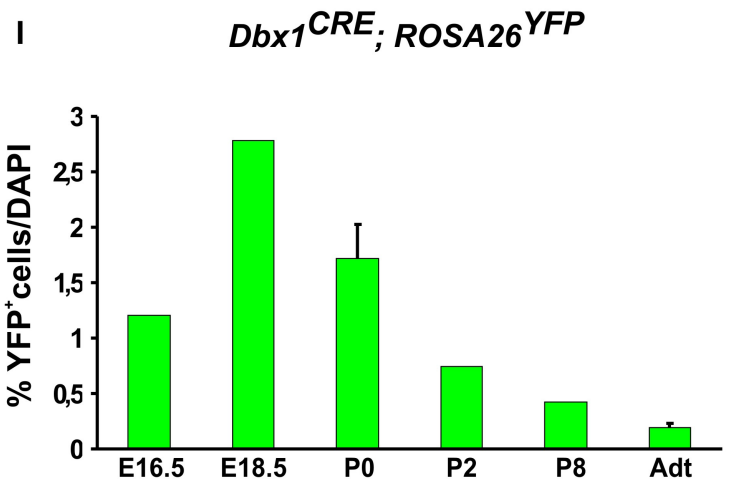

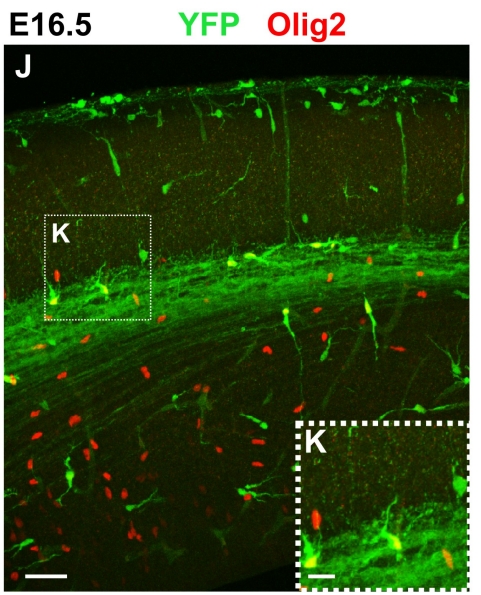

Teissier & al., Supplementary Figure 3

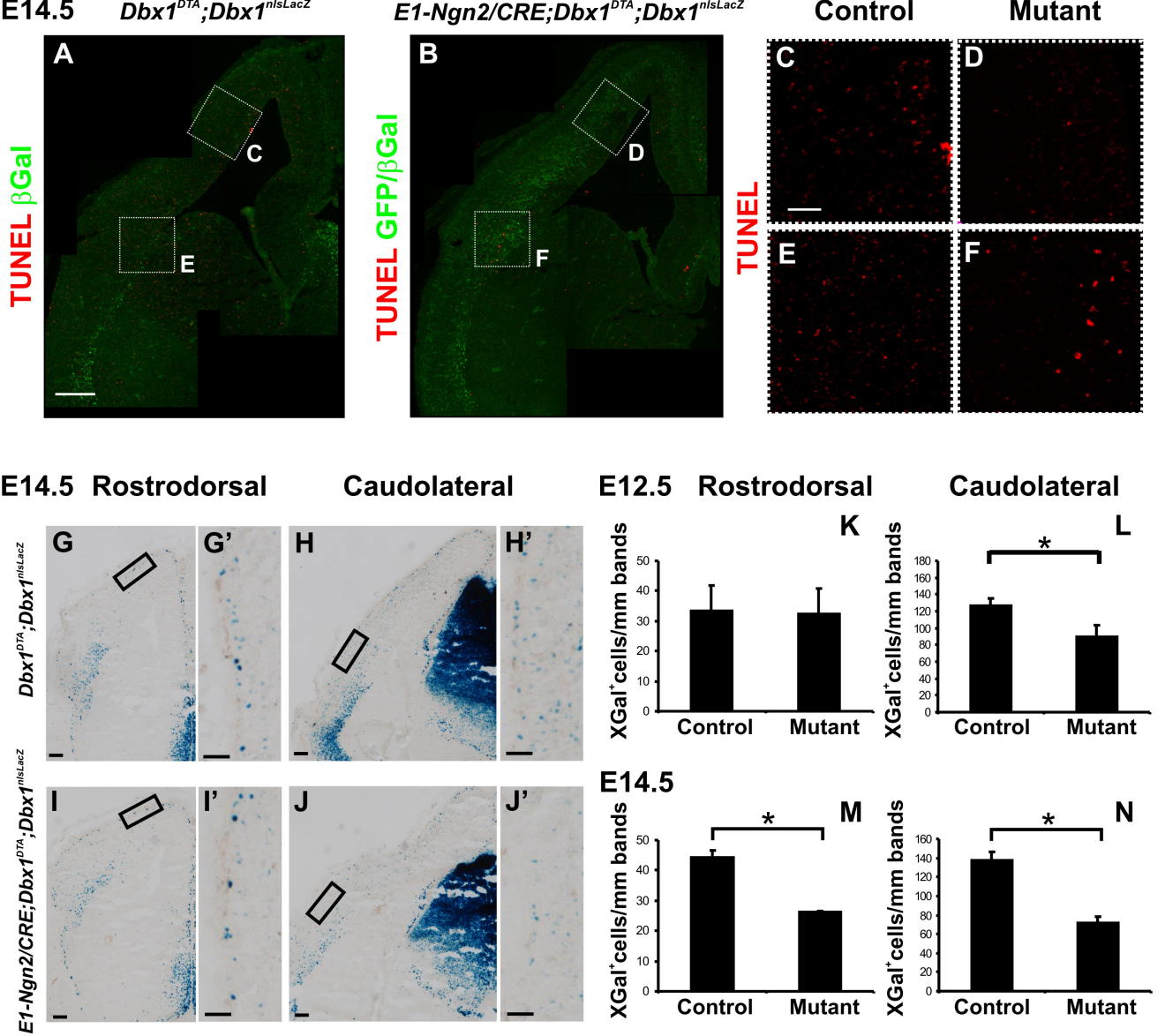

Teissier & al., Supplementary Figure 4

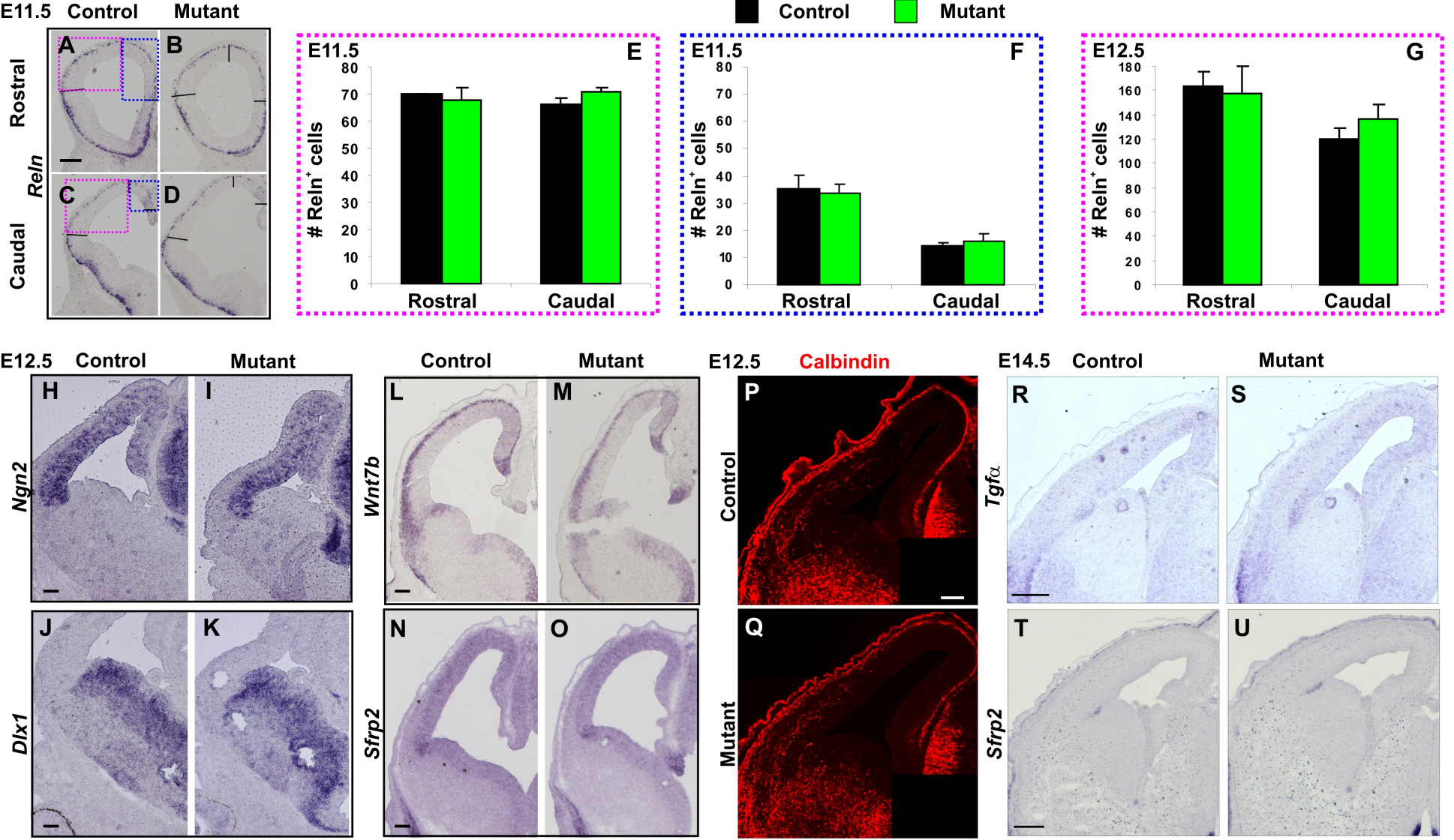

Teissier & al., Supplementary Figure 5

Supplementary Table 1 : Values of βGal^{+}Tbr1^{+}Reln^{-} cells per mm of CP

E13.5	Medial	Dorsal	Dorsolateral	Lateral
c0	0.93±1.14	8.6±0.94	26.60±2.40	54.42±5.25
c1	1.70±1.35	17.32±0.94	29.72±2.40	52.04±3.96
c2	2.20±1.35	18.877±4.86	24.28±6.65	50.49±2.57
c3	6.36±3.29	12.16±5.15	33.02±6.39	62.11±11.49
E14.5	**Medial**	**Dorsal**	**Dorsolateral**	**Lateral**
c0	27.37±2.31	40.23±7.12	44.23±5.09	32.54±14.98
c1	25.05±4.17	41.64±2.58	31.20±0.59	44.71±1.28
c2	19.92±3.05	27.98	28.52±3.63	42.54±1.51
c3	39.89±0.32	47.59	49.21±5.78	42.19±2.96

βGal^{+}Tbr1^{+}Reln^{-} neurons were counted on 4 coronal sections homogeneously distributed along the rostrocaudal axis and subdivided into 4 regions distributed along the mediolateral axis of the cortical plate of E13.5 (n=353) and E14.5 (n=448) on *Dbx1*^{CRE};*Tau*^{GFPireslacZ} animals. The table recapitulates the mean±sem of the number of cells in the thickness of CP per mm which have been reported as grey values for the schematic representations (See Materials and Methods).